JOURNAL OF GEOPHYSICAL RESEARCH: SPACE PHYSICS, VOL. 118, 5919–5930, doi:10.1002/jgra.50511, 2013

Long-period prompt-penetration electric fields derived from CHAMP satellite magnetic measurements

C. Manoj,[1,2] S. Maus,[1,2] and P. Alken [1,2]

Received 4 March 2013; revised 24 June 2013; accepted 12 August 2013; published 11 September 2013.

[1] The prompt penetration of the interplanetary electric field to the equatorial ionosphere is conveniently modeled with a frequency-dependent transfer function. However, long-period responses (>3 h) of previously estimated transfer functions differ considerably due to insufficient ionospheric eastward electric field (EEF) data useful for spectral analysis. The EEF derived from the Challenging Minisatellite Payload (CHAMP) satellite provides a new opportunity to reliably estimate the long-period transfer function for the first time. Our objectives in this paper are twofold: first, we analyze the frequency spectra of the equatorial ionospheric eastward electric field for periods greater than 6 h; second, we test the hypothesis that the average prompt-penetration effect lasts less than 3 h after an initial perturbation in the interplanetary electric field (IEF). We find that atmospheric sources dominate the EEF at diurnal frequencies, and its subharmonics and magnetospheric sources dominate the EEF for other frequencies. The CHAMP-derived transfer function has smaller errors than the previous estimates, and we confirm that the average prompt-penetration response of the equatorial ionospheric electric field to a 1 mV/m change in the IEF is negligible after 3 h and up to the maximum analysis period of 32 h. We update our transfer function model with the new data sets and make the filter coefficients available to the scientific community. The transfer function prediction matched reasonably well with the EEF observation in both the South American and Indian sectors. A transfer function model of the prompt-penetration effects, driven by the interplanetary electric field, can be highly beneficial to the real-time specification of the ionosphere.

Citation: Manoj, C., S. Maus, and P. Alken (2013), Long-period prompt-penetration electric fields derived from CHAMP satellite magnetic measurements, *J. Geophys. Res. Space Physics*, *118*, 5919–5930, doi:10.1002/jgra.50511.

1. Introduction

[2] In the daytime equatorial ionosphere of the Earth, the wind-driven currents coupled with the Earth's primarily horizontal magnetic field produce the equatorial eastward electric field (EEF). The EEF is the primary driver for several important features of the equatorial ionosphere, such as the equatorial ionization anomaly. The EEF is known to be highly variable from day to day, primarily as a result of the neutral winds coming from below and, additionally, due to solar wind electric fields penetrating from high latitudes to the equator. *Nishida* [1968] was the first to report the coupling between the interplanetary magnetic field and the equatorial ionospheric electric field. This strikingly linear relationship is understood to be caused by the penetration of the interplanetary electric field (IEF) to the equatorial ionosphere. The response of the equatorial ionospheric eastward electric fields to the variations in the IEF has been examined case by case and by statistical analysis [e.g., *Huang et al*., 2005; *Kelley et al*., 2003; *Huang et al*., 2007]. During geomagnetically quiet times, the low-latitude magnetosphere is shielded from the solar wind–induced disturbances at high latitudes by the Alfvén layer—an electrical charge buildup at the inner edge of the magnetospheric ring current. Based on theoretical studies, *Vasyliunas* [1972] predicted that this shielding is frequency dependent. Later, from a spectral study of the ionospheric electric field, *Earle and Kelley* [1987] showed that the Earth's magnetosphere acts as a high-pass filter allowing IEF fluctuations whose periods are less than a few hours to pass through to the inner magnetosphere.

[3] The power spectral density of the interplanetary electric field is directly proportional to the period of fluctuation. Recently, *Nicolls et al*. [2007], *Manoj et al*. [2008], and *Manoj and Maus* [2012] have shown that at the equatorial ionosphere, the IEF frequency band gets narrower to a broad peak around 2 h. This frequency-dependent relation between the IEF and the EEF can be used to develop a transfer function between them. While the transfer function relation describes the prompt-penetration effect on a majority of the days, the prompt-penetration effect can become unpredictable during very large geomagnetic storms. In such conditions, the magnetosphere-ionosphere coupling can be markedly different from the moderate storms, which occurs

[1]CIRES, University of Colorado Boulder, Boulder, Colorado, USA.
[2]NOAA/NGDC, Boulder, Colorado, USA.

Corresponding author: C. Manoj, CIRES, University of Colorado Boulder, 325 Broadway, Boulder, CO 80305, USA. (manoj.c.nair@noaa.gov)

2169-9380/13/10.1002/jgra.50511

more frequently. The transfer function allows for the prediction of EEF from IEF data. *Manoj et al*. [2008] has shown that a transfer function–based model can predict about 30% of the nonclimatological variations in the EEF. The longevity of the prompt-penetration effect is still highly contested. From morphological studies of the ionospheric electric fields, *Huang et al*. [2005] and *Kelley et al*. [2003] suggested that the prompt-penetration effect due to a perturbation in the IEF lasts longer than 3 h. *Manoj et al*. [2008] showed from an analysis of 8 years of IEF and Jicamarca Unattended Long-term Investigations of the Ionosphere and Atmosphere (JULIA) data that the prompt-penetration effect has a broad peak around 2 h periodicity followed by decay. This confirms a previous study by *Nicolls et al*. [2007] using the magnetometer data from Peru. However, the uncertainty in the long-period part of power spectral density hinders the ability to answer the question on the longevity of the average prompt-penetration effect in the EEF. For example, the *Nicolls et al*. [2007, Figure 7] model shows that the ionospheric response to an IEF step function has a nonnegligible signal (about 30% of the peak strength) even after 5 h of the initial perturbation. However, in the *Manoj et al*. [2008] model, the EEF response quickly decays, and there is no significant response in the EEF after 3 h of the IEF perturbation. The importance of this question cannot be understated, as a significant part of the variations in the ionospheric electric field can be attributed to the prompt-penetration effects. As a primary driver of several important features of the equatorial ionosphere, the EEF forms a critical input to models that predict ionospheric disturbances in real time. A continuous prediction of the equatorial ionospheric electric field for all longitudes is a primary requirement for such efforts. However, continuous ground-based measurements of the zonal electric field are sparse. *Manoj and Maus* [2012] reported a real-time prediction service for the EEF at all longitudes using a transfer function model driven by the Advanced Composition Explorer (ACE) data. Models of the equatorial ionospheric electrodynamics, such as the Coupled Thermosphere Ionosphere-Plasmasphere Electrodynamics model [for reference, see *Maruyama et al*., 2005], make use of the real-time EEF prediction service.

[4] Fourier-based spectral analysis is a powerful tool to study the quasiperiodic fluctuations in the interplanetary electric field and the correlated variations in the equatorial ionosphere [*Earle and Kelley* 1987; *Nicolls et al*., 2007; *Manoj et al*., 2008]. In order to generate smooth and statistically reliable spectral quantities, it is important to average the observations over a large number of samples. However, continuous measurements (greater than 10 h at a time) of equatorial electric fields suitable for Fourier analysis are rare. While Jicamarca Incoherent Scatter Radar data are available continuously for several hours (often extending to days), they operate on campaign modes, and such campaigns are infrequent. Additionally, the gaps in the data, often extending to several hours due to system breakdowns, make it unsuitable for Fourier-based analyses. Due to these limitations in the availability of EEF data, spectral analyses of the EEF for periods greater than 10 h were nearly impossible. *Earle and Kelley* [1987] used the Jicamarca radar data to estimate the power spectra of the equatorial ionospheric eastward electric field (EEF) in the period range 1–10 h. During the geomagnetically active days (when the planetary geomagnetic index, *Kp*,was greater than about 3), they found that the magnetospheric sources dominate the atmospheric sources in the EEF data. However, the power spectral densities for periods above 6 h were poorly resolved due to fewer cycles available per time series segment. *Nicolls et al*. [2007], using the magnetometer data from Peru, estimated the EEF spectra for periods of 0.03–10 h. While the magnetometer data are available for a large number of days, the length of continuous segments is limited to 10 h or less during the daytime. The magnetometer data have the additional problem of low sensitivity to the EEF in the early morning and evening hours (due to the weak equatorial electrojet currents), further limiting its useful length. Due to these limitations, to our knowledge, the spectra of the EEF signals were not studied for periods greater than 6 h. In addition to the study of the frequency-dependent penetration of solar wind electric fields, the spectra of the EEF also are useful to identify various sources that contribute to it. For example, some EEF sources are periodic (such as neutral wind–induced ionospheric dynamo system), some are pure random (such as disturbance dynamo system), and some are highly correlated to the solar wind variations (such as the prompt-penetration signals). The most convenient way to separate these sources is by studying their frequency spectra.

[5] The EEF data derived from the Challenging Minisatellite Payload (CHAMP) satellite offer a unique data set to study the long-period fluctuations in the EEF that is correlated to the changes in the interplanetary electric field. Launched in July 2000 into a circular, near-polar orbit at 456 km altitude [*Reigber et al*., 2002], the satellite performed highly accurate measurements of the Earth's magnetic field until its reentry to the atmosphere in September 2010. When CHAMP crosses the dip equator on the dayside, it measures a latitudinal magnetic profile of the equatorial electrojet (EEJ) signature [*Lühr et al*., 2004]. *Alken and Maus* [2010] estimated the daytime EEF from the CHAMP EEJ observations for all longitudes and daytime local times (LTs). They reported a very high correlation (0.84) between EEFs derived from CHAMP and from the JULIA coherent scatter radar at Jicamarca, Peru. This data set, which spans 2000–2009, contains nearly 50,000 EEF data points and thus offers a new possibility to study the long-period (periods above 10 h) fluctuations of the EEF. This is because the satellite completes an orbit every 92 min and decreases 1 h in local time every 11 days. Hence, the CHAMP-derived EEF offers an unprecedented opportunity to study the long-period prompt-penetration effect in the EEF.

[6] This leads to the two main objectives of the paper. The first is to present—for the first time—the spectra of the equatorial ionospheric electric fields for periods greater than 10 h. Using a combination of observations from ground and space, we investigate the spectral properties of the interplanetary electric field and the equatorial ionospheric electric fields for periods from 10 min to 512 h. This will enable us to answer the following questions: (1) What are the primary sources of the EEF signals for fluctuations with a periodicity longer than 6 h? (2) How differently do these sources influence the EEF during geomagnetically active and passive periods? (3) How long does the average prompt-penetration effect last in the EEF after a perturbation in the IEF? We also take this opportunity to update our prompt-penetration

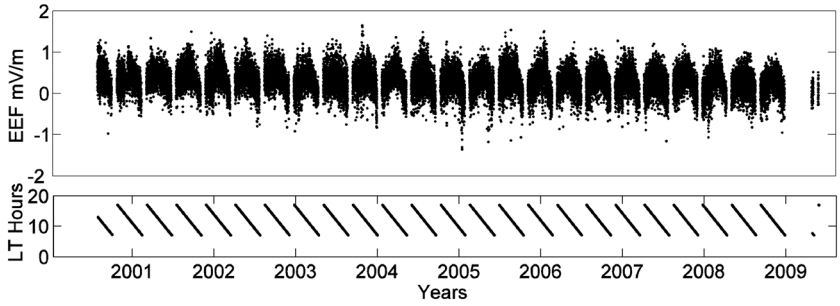

Figure 1. The Equatorial ionospheric electric field data derived from CHAMP magnetic measurements. The data contain all the longitude and seasons.

model [*Manoj et al*., 2008] with the EEF data from the CHAMP satellite.

[7] We discuss the data sets and their processing in section 2. The spectral properties of the interplanetary and equatorial ionospheric electric fields are discussed in section 3. We develop a transfer function between the interplanetary and equatorial ionospheric electric fields and discuss two case studies in section 4. In section 5, we discuss the implications of our results. Section 6 summarizes our findings. We demonstrate in Appendix A the recovery of the transfer function and its errors from realistic mock data sets of the interplanetary and equatorial ionospheric electric fields.

2. Data and Processing

2.1. CHAMP-Derived Equatorial Ionospheric Eastward Electric Field

[8] The EEFs were obtained from the individual CHAMP equatorial passes for all longitudes and seasons during the years 2000–2009. For each daytime equatorial pass between 7 and 17 local time (LT), the electrojet current strength was deduced from the scalar magnetic data using a procedure detailed in *Lühr et al*. [2004]. The EEF for each pass was estimated from the EEJ current strength following the procedure detailed in *Alken and Maus* [2010]. The magnetic effects from the satellite altitude and from the various *F* region plasma effects are accounted for in this approach. Hence, we do not expect our results to be biased from the systematic changes in the satellite's orbit or the ionospheric environment. *Alken and Maus* [2010] reported a correlation coefficient of 0.84 between the electric field estimates from CHAMP with that of the JULIA radar with a slope parameter near to unity. In a previous study in the Indian sector, *Manoj et al*. [2006] found a correlation coefficient >0.9 when the CHAMP-derived EEJ strength was compared with the electrojet magnetic signals. These high correlations of CHAMP data with the ground station give us high confidence on its EEF estimates.

[9] Figure 1 shows the entire EEF time series from nearly 50,000 CHAMP crossings considered for the study. The most striking feature in the plot is the LT-dependent variation of the EEF. This is because of the climatological variations of the EEF as CHAMP progresses slowly in LT. The daytime EEF is mostly positive (eastward), and the negative occurrences of EEF are generally limited to morning and evening hours. Figure 1 (second panel) shows the LT progression of CHAMP with respect to UT. The gaps in the data reflect the absence of EEJ signal between 17 and 7 LT.

[10] There are two important aspects of CHAMP data that we must consider when we treat it as a time series. Unlike the stationary observatories, the time series derived from the CHAMP satellite are asynoptic sampling (measurement taken at a single location at a given time) of the EEF. CHAMP moves $-23°$ in longitude when it revisits the daytime equator. A number of recent publications [for example, *Lühr et al*., 2012] report the longitudinal structures in the equatorial electrojet and electric fields. Hence, the spatial signals in the EEF get folded in to the frequency spectrum. However, this signal is uncorrelated with the interplanetary electric field. In Appendix A, we demonstrate that our spectral averaging method can reliably recover the transfer function and its errors between the IEF and EEF data in the presence of significant uncorrelated noises.

[11] The second issue is that the CHAMP satellite undersamples the EEF variation. This effect, known as "aliasing" in spectral analysis, arises due to the presence of a frequency content higher than the Nyquist frequency (half the sampling frequency) in the EEF. CHAMP revisits the dayside equator in about 92 min, but the EEF shows strong variability with periodicities of less than 92 min [e.g., *Earle and Kelley*, 1987]. The end effect is that the power of signals with periodicities of less than 90 min will be folded back into longer periods. The natural spectrum of EEF fluctuations increases with the period, generally gaining 2 orders of magnitude on 1 order of frequency. Because of this special situation, the aliasing should be only a serious problem for frequencies above one-half the Nyquist frequency. While discussing the measurement errors of the interplanetary magnetic field (IMF) due to aliasing, *Russell* [1972] also arrived at the same conclusion. In Appendix B, we demonstrate this aliasing effect using synthetic EEF data. The errors due to aliasing in the CHAMP EEF are hence expected to affect only periods of less than 6 h.

2.2. EEF Data From Ground-Based Measurements

[12] The eastward electric field in the daytime equatorial ionosphere for the South American sector is obtained from JULIA measurements. The JULIA radar is located at the Jicamarca Radio Observatory, Peru (11.95°S, 76.8°W). *Hysell et al*. [1997] described the instrument and first results from JULIA. The JULIA radar observes the so-called 150 km echoes [*Kudeki et al*., 1993] and the corresponding vertical Doppler velocity. The data are recorded with a 5 min sampling interval during daytime. Our analysis is based on 1002 days of JULIA drift data available between 2000 and 2008. We calculate the eastward electric field from JULIA

Table 1. The Power Spectral Density of the IEF and the EEF Were Averaged Over a Number of Observations[a]

	Length (h)	Number of Segments $ap > 20$	Number of Segments $ap < 20$
IEF (OMNI)	512	44	332
EEF (JULIA)	6	45	222
EEF (CHAMP)	512	11	40

[a]The table gives the numbers and lengths of the individual data sets considered.

*Vz*measurements by applying the formula $E = -Vz \times B$, where *Vz* is the vertical drift in *meters per second*, and *B*is the magnetic field strength at the Jicamarca site [*Kelley*, 1989].

[13] For case studies, the eastward electric field for the Indian sector is derived from the horizontal intensities of the magnetic field observed at an electrojet (Tirunelveli—TIR) and at a nonelectrojet (Alibag—ABG) magnetic observatory. By taking the difference between the horizontal strengths at the electrojet and nonelectrojet stations, the magnetic contributions from the magnetospheric ring current and the global "Sq" (solar quiet) current can be removed [*Manoj et al*., 2006]. The residual magnetic field (called "ΔH") is known to be highly correlated with the equatorial ionospheric electric field on the dayside [*Anderson et al*., 2004]. We follow the technique described by *Anderson et al*. [2004] to derive the zonal electric field from magnetic field measurements.

2.3. Interplanetary Electric Field Data

[14] To determine the IEF, we use the IMF and solar wind velocity data from the Advanced Composition Explorer (ACE) satellite and the Global Geospace ScienceWIND satellite both located at the L1 Lagrangian point. The data are obtained from the OMNI website (http://omniweb.gsfc.nasa.gov) and are sampled every 5 min. Assuming that the solar wind is due to the *ExB* drift of the interplanetary magnetic and electric fields, IEF *Ey* and *Ez* components are calculated as $Ey = -Vx \times Bz$, where *Vx* is the solar wind velocity, *Bz* is the vertical component of the interplanetary magnetic field, and *Ey*is the dawn-dusk component of the IMF. The vectors are relative to the geocentric solar magnetospheric coordinate system. The *x* axis is along the Sun-Earth line with the origin at the Earth, and *x* is positive toward the Sun. The *y* axis is the cross product of the Earth's dipole axis and the *x* axis and is positive toward dusk. The *z* axis is perpendicular to the *xy* plane and is positive to the Earth's magnetic north. The OMNI data set is primarily intended to support studies of the effects of solar wind variations on the magnetosphere and the ionosphere and is time shifted by the OMNI group to the magnetosphere's bow shock nose from the location of the satellites. For a detailed description of the processing, visit the OMNI website (http://omniweb.gsfc.nasa.gov/html/omni_min_data.html).

3. Spectral Properties of the Electric Fields

3.1. Electric Field Spectra for the EEF

[15] From a large sample, it is possible to generate smooth and statistically significant spectral information of the electric field data. Our objective in generating these smooth spectral density estimates is twofold: (1) to present, for the first time, the spectral density of the EEF in the period range 10–512 h and (2) to separate the prompt-penetration signals in the EEF data. For periods up to 6 h, we use the JULIA data, and for longer periods, we use the CHAMP data. We divide the data sets into geomagnetically active and passive periods defined by whether the mean *ap* index is above or below 20. The three-hourly *ap* index ranges from 0 to 400 and is derived from the planetary geomagnetic index, *Kp*. The power spectral densities of the data are found following the popular method by *Welch* [1967]. This is done by doing the following: (1) dividing the IEF and EEF time series into "*n*" segments, (2) computing the Fourier transforms of the individual segments after applying a "Hanning" window, and (3) averaging these quantities over the segments to calculate the correlations in the frequency domain. The number of individual data segments used in the averaging process is given in Table 1. It is advantageous to divide the time series into *n* overlapping segments since it reduces the standard deviation of the result by a factor of $1/\sqrt{n}$. The power spectral densities of the equatorial ionospheric electric field data are plotted in Figure 2.

[16] Of particular interest is the increase in the power of spectra with period (or decrease with frequency). The so-called $1/f^{\alpha}$ noise is found in many natural systems [*Kirchner*, 2005], where *f* is the frequency. The scaling exponent α is typically estimated from the log-log slopes of their Fourier power spectra. The EEF spectra presented in Figure 2 have a log-log slope of about −2. This implies that the EEF spectra generally gain 2 orders of magnitude on 1 order of period. The data for the periods greater than 6 h come from the CHAMP measurements. To our knowledge, this is the first time that the ionospheric electric field spectra are estimated up to periods as long as 512 h. The smoothness of the spectra between 1 and 6 h and between 30 and 512 h is due to a decreased spectral resolution (on a logarithmic scale) which causes the power in the adjacent frequencies to get averaged.

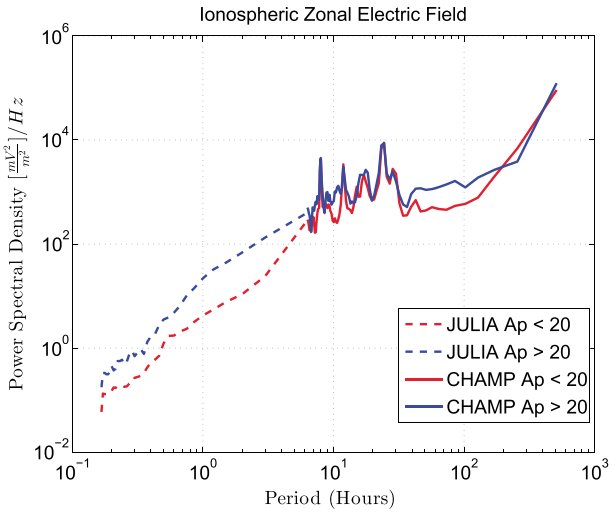

Figure 2. The power spectral density plot of the zonal electric field data. The dashed lines represent the data from radar (JULIA) measurements, and the solid lines represent the data from satellite (CHAMP) measurements.

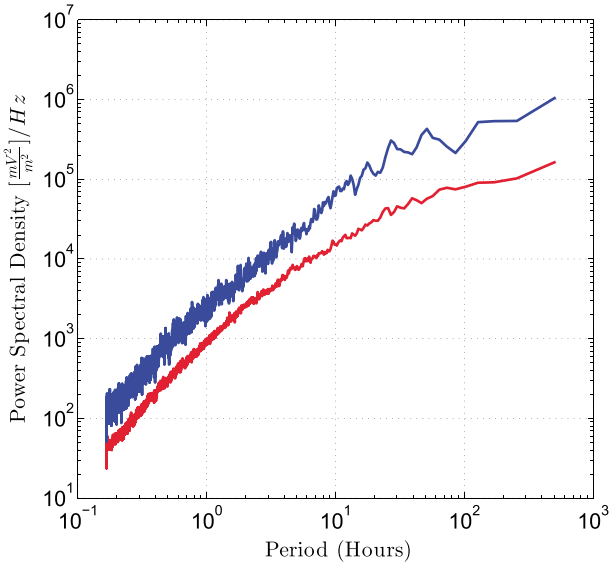

Figure 3. The power spectra of IEF. The blue line shows spectra for the time duration when $ap > 20$. The red line shows the spectra when $ap < 20$.

There is no offset between the CHAMP and JULIA spectra. Considering the vast differences in the measurement and processing of data from the JULIA radar and the CHAMP satellite to estimate the EEF, their excellent alignment validates the derivation of the EEF from the CHAMP magnetic measurements. For periods greater than 6 h, distinct spectral peaks at periods of 8, 12, 16, and 24 h are superimposed on the background power. While the background power in the spectra is higher during the geomagnetically active periods, the amplitudes of the peaks remain unchanged. The electric field spectra show no consistent features beyond 24 h periods, and the variations in this region probably reflect the random occurrence of ionospheric disturbances. The power of the spectra increases in both curves toward our maximum period of 512 h.

3.2. Electric Field Spectra for the IEF

[17] We plot the power spectral density of the IEF *Ey* in Figure 3. Power spectral densities from individual, time series (each 512 h long) segments of the IEF during the years 2000–2009 were averaged following the method we used for the EEF. The power spectra during magnetically active periods ($ap > 20$) are about half an order of magnitude higher than that during magnetically quiet time. At high levels of geomagnetic activity, the time variations in the EEF are enhanced at all the frequencies. The enhancement is not apparent at the tidal periods where the background EEF signals are dominated by the tidal variations. This is inconsistent with a similar analysis of IEF spectra carried out by *Nicolls et al.* [2007]. The power spectra of the interplanetary magnetic field are known to have a log-log slope of about −5/3 in the period range of 10 min to 4 h [*Li et al.*, 2011; *Sari and Ness*, 1969]. The slope of the IEF power spectral density closely follows that of the interplanetary magnetic field (IMF). The IMF power spectrum shows a constant slope of about −5/3 below a period that decreases with the heliocentric distance [*Meyer-Vernet*, 2007]. At the L1 point, where the IEF data are observed, this period is approximately 3 h [*Meyer-Vernet*, 2007]. Above this period, the IEF spectra start to flatten.

3.3. Coherence Between the IEF and the EEF

[18] For joint analysis of the IEF and EEF data, we divide the whole period range into two. For the period range of 10 min to 6 h, we use the JULIA EEF and the OMNI IEF (both sampled at 5 min intervals). For the period range of 6–32 h, we use the CHAMP EEF and the OMNI IEF (both resampled every 2 h). As we will show in the subsequent part of this paper, the fluctuations in the IEF and EEF are very weakly correlated for periods above 10 h, so it is appropriate to limit the maximum period to 32 h. By limiting the segments to shorter lengths, we have more samples available for spectra averaging. While this reduces the frequency resolution of the spectra, as we show in Appendix A, it is important to average the spectral quantities over a sufficient number of samples to minimize the effect of uncorrelated noises in the EEF. For periods from 10 min to 6 h, we follow the method described in *Manoj et al.* [2008] to derive the coherence and transfer functions. The only difference here is that we restrict the analysis to the time durations when the mean *ap* is greater than 20. We treat the data for the period range of 6–32 h as follows. We restrict the analysis to durations where the mean *ap* index is greater than 20. We time delay the IEF data by 17 min to account for their travel from the magnetosphere's bow shock nose to the equatorial ionosphere [*Manoj et al.*, 2008]. The Fourier-based analysis requires that the individual data segments should be continuous. We low-pass filter the IEF data to minimize aliasing of power from periods less than 2 h into the frequency spectrum. We downsample the IEF data from a 5 min interval to every 2 h. Then, we divide the data into 32 h long segments. We discard an IEF segment if either of these two tests passed in the corresponding raw data: (1) a segment has more than two consecutive missing points (>10 min) or (2) if more than 10% of the data points are missing. The gaps within a segment are filled by linear interpolation.

[19] We remove the climatological variations from the EEF data using the *Alken and Maus* [2010] model and restrict the EEF data to a local time interval of 9–15 h. The original EEF time series with a median sampling interval of 91.9 min (time taken by CHAMP to revisit the dayside equator) is interpolated every 2 h at the exact time stamps of the IEF data segments. We discard any EEF segments with a data gap. As we have discussed before, we limit the CHAMP-derived spectral values to a minimum of 6 h periodicity to avoid the possible effect of aliasing from the periods lower than 92 min. Due to these stringent requirements we imposed, the number of coincident IEF and EEF segments available to the study was 321.

[20] The magnitude squared coherence (hereinafter called "coherence") estimates the fraction of the EEF variance that is correlated with the IEF as a function of frequency. We calculate the coherence as

$$C_{\text{IEF-EEF}}(f) = \frac{|P_{\text{IEF-EEF}}(f)|^2}{P_{\text{IEF}}(f)P_{\text{EEF}}(f)}, \quad (1)$$

where $C_{\text{IEF-EEF}}$ is the magnitude squared coherence, $P_{\text{IEF-EEF}}$ is the cross-spectra between the IEF and the EEF, P_{IEF} is the autospectra of the IEF, P_{EEF} is the autospectra of the

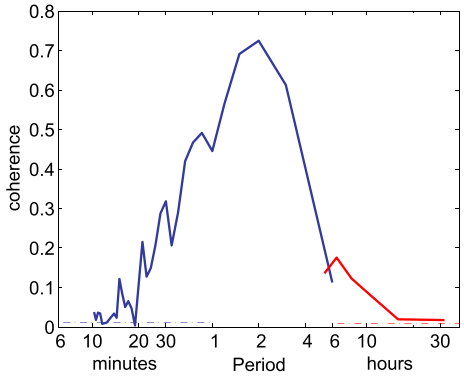

Figure 4. Coherence between IEF and EEF when *ap* is greater than 20. The blue line shows the coherence between IEF and JULIA-derived EEF, and the red line shows the coherence between IEF and CHAMP-derived EEF. The dashed lines indicate an error level for the coherence estimations.

EEF, and *f* indicates the frequency. The cross-spectra and the autospectra of the IEF and the EEF were individually estimated and then averaged. The coherence values were estimated from these average spectral densities following equation 1. Figure 4 shows the coherence between the IEF and the EEF for periods between 10 min and 32 h. As shown previously by *Manoj et al*. [2008], the coherence between the IEF and the EEF peaks around 2 h. The CHAMP-derived EEF show low coherence with IEF data (red lines). However, the CHAMP data show smooth transition in coherence from the longest period estimated from JULIA. While the coherence for periods >6 h is low (lower than 0.2), the values are still statistically significant. The horizontal broken lines to the bottom of the curves show a measure of the significance level of coherence [*Thompson*, 1979]. This line gives an error level below which the coherence values are unreliable.

4. Transfer Function Between the IEF and the EEF

4.1. Transfer Function and its Errors

[21] The frequency-dependent transfer function between the interplanetary electric field (input) and the equatorial ionospheric electric field (output) is determined as the ratio of the cross-spectra to the autospectra following *Swanson* [2000], i.e.,

$$T_{\text{IEF-EEF}}(f) = \frac{P_{\text{IEF-EEF}}(f)}{P_{\text{IEF}}(f)}, \tag{2}$$

where $T_{\text{IEF - EEF}}$ is the transfer function between the IEF and the EEF. The transfer function is, in general, complex, and both its magnitude and phase provide useful information. This estimated transfer function only takes into account the linearly correlated proportion of the EEF with the IEF. This fundamental strength of the transfer function method is particularly suitable for predicting the EEF signals since a significant part of the variations in EEF and IEF is uncorrelated. For example, the disturbance dynamo fields [e.g., *Scherliess and Fejer*, 1999] in the EEF, which are not linearly correlated to the IEF, will be treated as noise and hence cannot influence the transfer function.

[22] The signal-to-noise ratio between the IEF and the EEF is calculated from the coherence as

$$\text{SNR}(f) = \sqrt{\frac{1 - C_{\text{IEF-EEF}}(f)}{C_{\text{IEF-EEF}}(f)}} \tag{3}$$

[23] The transfer function error amplitude is then calculated by following *Swanson* [2000], i.e.,

$$E_{\text{IEF-EEF}}(f) = \sqrt{\frac{1 - C_{\text{IEF-EEF}}(f)}{2n\, C_{\text{IEF-EEF}}(f)}}\, |T_{\text{IEF-EEF}}| \tag{4}$$

where *n* is the number of segments averaged. The inclusion of *n* in the equation above helps to define a confidence interval around the transfer function amplitude. It is clear that if coherency drops, the error of the transfer function increases. The formulation for the error assumes that the input data (IEF) is error free, and hence, it reflects the error contribution from the EEF to the transfer function. In the real world, however, there are errors both in input and output measurements. However, it is reasonable to assume that the in situ measurements of the IEF by the ACE/WIND satellites contain less error than the remotely measured EEF data.

4.2. Transfer Function Between the IEF and the EEF

[24] Figure 5 shows the magnitude of the transfer function between the IEF and the EEF for periods between 10 min and 32 h. The JULIA-derived transfer function is calculated from the same data set used by *Manoj et al*. [2008] by further restricting the data for which the *ap* index was greater than 20. The error bars show that the transfer function coefficients are best estimated for periods between 30 min and 4 h. The JULIA-derived transfer function shows a relatively larger error bar at 6 h, which is the longest period resolved. The CHAMP-derived transfer function (data limited to $ap > 20$) magnitude (red squares) has very small magnitudes for periods greater than 6 h. The CHAMP data are also in agreement with the decreasing trend shown by the JULIA data. The CHAMP-derived transfer function has less error than the error of the JULIA-derived transfer function at 6 h. The

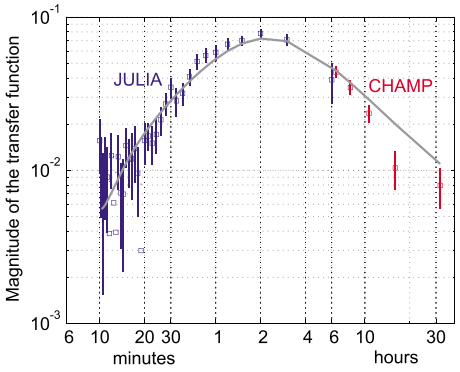

Figure 5. The estimated magnitudes and errors of the transfer function between the interplanetary and equatorial ionospheric electric fields are plotted as a function of periods. Blue indicates JULIA data, and red indicates CHAMP data. The response of the best fitting digital filter (grey) is also shown.

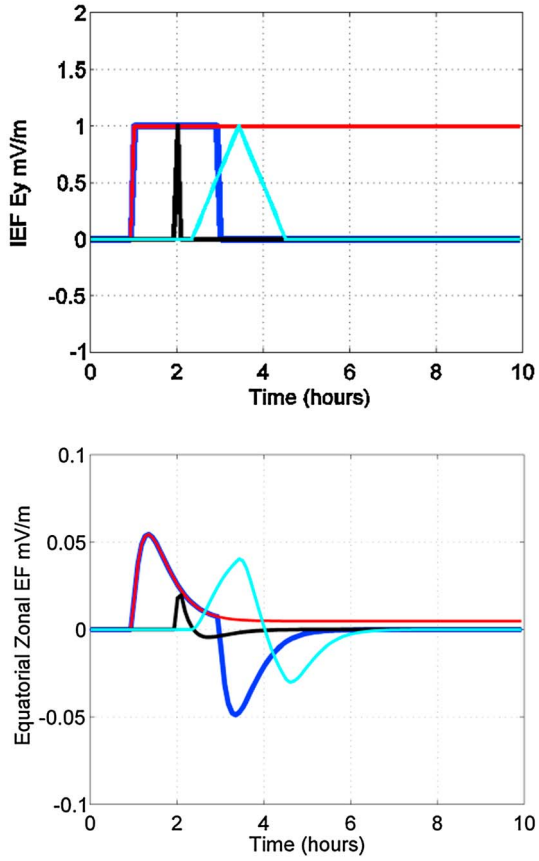

Figure 6. The response of the transfer functionto the synthetic inputs from IEF. The first panel shows the input signal, and the second panel shows the EEF output.

phase of the transfer function (not shown here) is very similar to that we presented in an earlier paper [*Manoj et al.*, 2008, Figure 6]. It is advantageous to convert the transfer function response to digital filter coefficients when applying the transfer function to the IEF time series. This allows for the estimation of the EEF in the time domain, without the need to do a fast Fourier transform. The filter coefficients were estimated minimizing the error between the transfer function magnitude and the predicted response of the filter in a least squares sense. The grey line in Figure 5 shows the response of the digital filter. The estimated filter coefficients are

$$a = [1.0, -0.586, -0.955, 0.63] \text{ and}$$
$$b = [0.018, 0.009, -0.018, -0.009].$$

[25] The above coefficients may be used to predict the EEF at time n with the filter difference equation [e.g., *Smith*, 2007]

$$y(n) = b_0x(n) + b_1x(n-1) + \cdots + b_Mx(n-M) - a_1y(n-1) - \cdots - a_Ny(n-N), \quad (5)$$

where x is the input IEF data, y is the EEF data, and N and M are the lengths of the coefficient vectors a and b minus 1. The present sample is denoted by n, and $n-1$ denotes the previous value. Note that the sampling interval for input and output is 5 min. Since this is a "feedback" filter, meaning the present EEF also depends on the past EEF values, it is a good practice to consider about 3 h worth of prior IEF data.

5. Discussion

5.1. Spectra of the EEF and the IEF

[26] The power spectral density of the EEF (Figure 2) is roughly orders less in magnitude than that of the IEF (Figure 3). Their slopes on the log-log scale are nearly the same. During the geomagnetically active period, the EEF data (Figure 2) show a "bulge" (deviation from its trend on the log-log plot) around 2 h. The IEF spectra do not show such a deviation from its general trend. This observation favorably compares with that by *Nicolls et al.* [2007]. When $ap > 20$, and for periods between 30 min and 2 h, the slope of the EEF spectra is significantly higher (almost -3) than that of the IEF. Above 2 h, the EEF spectra quickly return to the average background trend. This is also the period range where the IEF and the EEF are most coherent (Figure 3). We have previously interpreted this as the effect of the prompt-penetration of the IEF to the equatorial ionosphere [*Manoj et al.*, 2008]. From its peak value of 0.7 at 2 h, the coherence quickly decays on either side of the frequency spectrum. Both the CHAMP- and JULIA-derived coherence values are very similar in the period of about 6 h. While the coherence itself is small for this period, the values are statistically significant.

[27] The most dominant spectral peak in the EEF is at 24 h (Figure 2). Beyond 24 h, the spectra suddenly lose power. This is because the dominant 24 h periodicity gives power to numerous subharmonics in the EEF spectra. Parts of these amplitudes "leak" to the adjacent Fourier points and raise the background noise. There are two smaller peaks in the power spectra approximately at 29 and 42 h. We do not have an explanation for these peaks. From 48 to 512 h, the spectra show no preferable pattern. A similar observation is made by *Titheridge* [1973] when analyzing the amplitude spectrum of an ionospheric total electron content at a high-latitude observatory. The active day EEF spectrum is significantly higher than that during passive days in this period range. The most probable source of energy in this period range could be ionospheric disturbances related to magnetospheric variations. There is an increasing trend in the EEF power from about 200 to 512 h. This is probably due to the left flank of the 27 day (648 h) peak attributed to solar rotation [for example, *Mursula and Zieger*, 1996].

[28] Figure 2 indicates that while the background power is directly related to the geomagnetic activity level, the spectral peaks at 8, 12, 16, and 24 h are not. This means that the atmospheric sources dominate the EEF at these periodicities and that the magnetospheric sources dominate the EEF at periods in between the peaks. This is expected since the solar wind variations have a more direct effect on the disturbance electric field than on the ionospheric dynamo. Unlike the bulge in the EEF around 2 h, the spectral peaks between 8 and 24 h are not coherent with the IEF (Figure 4). We interpret these peaks as a result of the E region waves [e.g., *England et al.*, 2006] sampled by the CHAMP satellite. The stationary wave components in the E region appear at integer frequencies corresponding to their wave number. Migrating wave components, on the other hand, Doppler shifted to lower (higher) frequencies for westward (eastward) moving components [e.g., *Salby*, 1982] in the frequency spectra. A complete frequency–wave number analysis of the EEF is outside the scope of the present study.

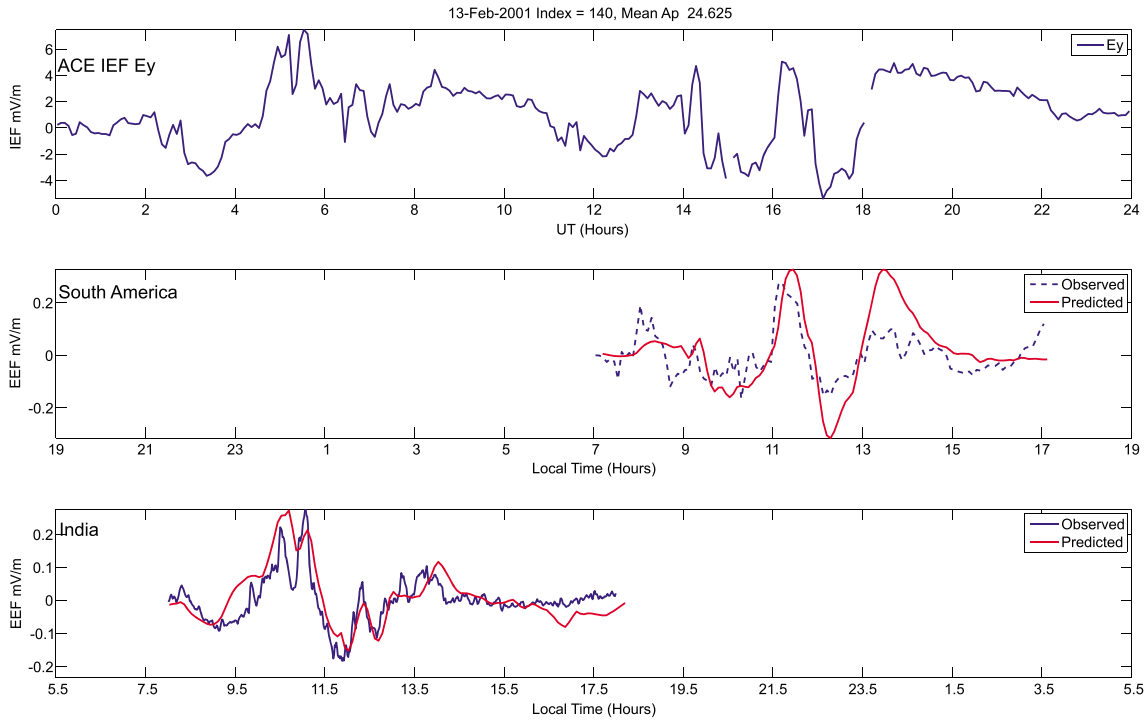

Figure 7. IEF and EEF data for 13 February 2001. The first panel shows the IEF *Ey* time shifted to account for the propagation delay. The red lines in the second and third panels show the transfer function–predicted EEF for the South American and Indian sectors. The observed data are given in blue.

[29] While interpreting the EEF spectra, one must note that the while the JULIA radar samples the ionospheric electric field over Jicamarca, the CHAMP EEF samples the EEF from all the longitudes. It then follows that a stationary observatory and a satellite will differently map the periodic signals (both stationary and travelling) in the ionosphere. We argue that electric fields with large spatial scales, such as the prompt-penetration signals, do not have such a problem. The fact that coherence values estimated from CHAMP and JULIA are comparable at 6 h supports our argument.

5.2. Transfer Function

[30] Figure 5 indicates that the CHAMP-derived transfer function (red squares) has comparable magnitudes with those derived from JULIA. Furthermore, the CHAMP data confirm the decreasing trend found in the JULIA-derived transfer function magnitudes for periods >2 h. These two findings are important since they remove an uncertainty in the JULIA-derived transfer function at about 6 h. The estimated error for the CHAMP transfer function at 6 h is less than that of the JULIA-derived transfer function—mainly due to the higher coherence between CHAMP and IEF at this period [see equation 4 and Figure 4].There are no data points between 3 and 6 h due to data limitations, and we impose a smooth transfer function in this period. The natural transfer functions are expected to be smooth functions of frequency. Larger error bars or significant misfit between JULIA and CHAMP at 6 h would have made the smooth fit between 3 and 6 h questionable. However, due to the relatively small errors of the transfer function for periods at and above 6 h, we have very high confidence on the imposed smooth transfer function. However, it has to be noted that our analysis removes all Fourier components above 32 h, so that variations in the IEF that might have measurable spectral power at larger periods are not represented in the transfer function. Our results are consistent with the previous estimates of the prompt-penetration transfer function by *Manoj et al*. [2008], but inconsistent with *Nicolls et al*. [2007], where they obtained a significant (30% of the peak value) transfer function response even 5 h after the IEF perturbation. However, both these studies have shown that the maximum efficiency of prompt penetration occurs for the fluctuations with periodicity around 2 h.

[31] The CHAMP EEF spectra show a series of peaks in a period range between 6 and 24 h where we estimate the transfer function. In Appendix A, we examine the effect of uncorrelated and deterministic noise on the estimation of the transfer function and its errors. With a realistic set of synthetic IEF and EEF data sets, we demonstrate that our spectral averaging method can reliably estimate the transfer function between the IEF and the EEF even in the presentence of uncorrelated noises.

5.3. Response of the Transfer Function Model to Synthetic Inputs

[32] We now demonstrate the response of the transfer function to simple forms of input IEF. Figure 6 shows the input IEF signals and the corresponding EEF response from the transfer function model. A positive step in the IEF with an amplitude of 1 mV/m produces an instantaneous EEF response with a maximum amplitude of ~0.05 mV/m. Note that in the actual application, the propagation delay for the IEF from the measurement site to the equatorial ionosphere should be added. Similarly, a step-down in the IEF also produces the effect in the EEF in the opposite direction. In both cases, the EEF response quickly loses its amplitude after the

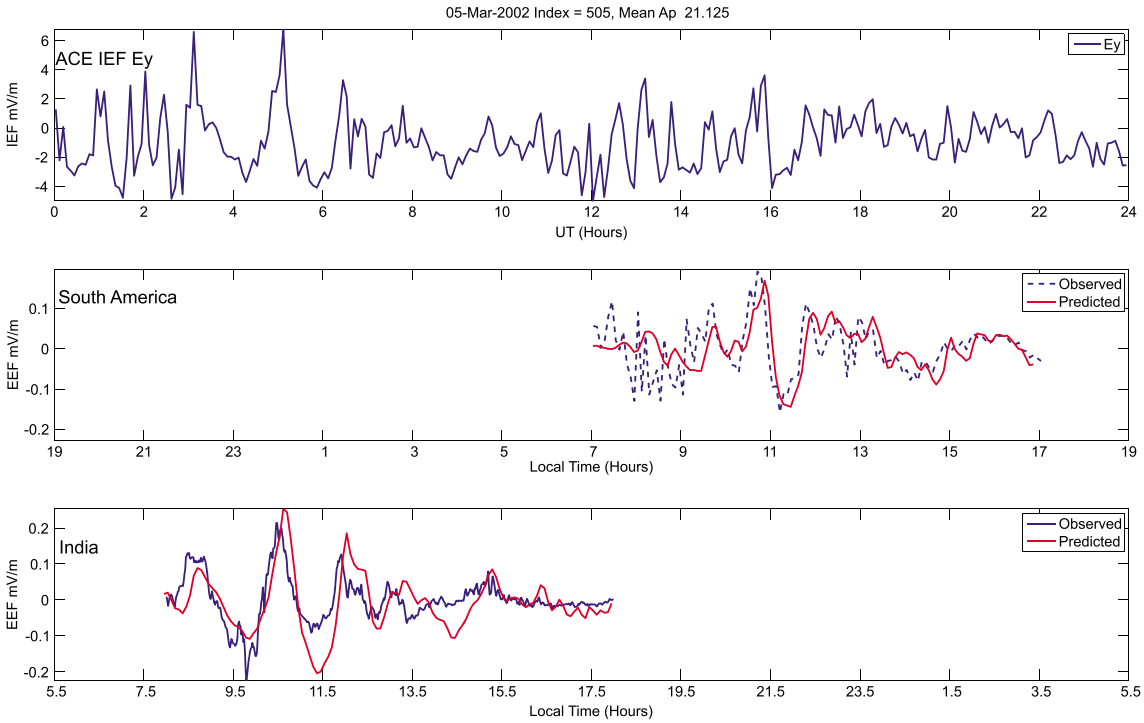

Figure 8. IEF and EEF data for 05 March 2002. The first panel shows the IEF *Ey*, time shifted to account for the propagation delay. The red lines in the second and third panels show the transfer function–predicted EEF for the South American and Indian sectors. The observed data are given in blue.

initial perturbation. This shows that the transfer function model is only sensitive to the time changes in the IEF. Another interesting feature of the model is the difference between the output amplitudes for a spike and a triangular function of IEF. The triangular function, which spans 2 h, produces a larger EEF response than the spike (5 min duration). The transfer function allows the quasisinusoidal fluctuations of IEF with a periodicity of a few hours to pass through it while damping the high-frequency signals such as a spike. In all these cases, the responses of the EEF become negligible after 3 h from the end of the IEF perturbation. This result confirms a similar observation by *Manoj et al*. [2008] based only on the JULIA radar data. We wish to point out that our statistical results do not necessarily contradict earlier case studies such as *Huang et al*. [2005]. In these works, the IEF creates a bias in the EEF that persists for hours, an effect which is difficult to reproduce with the transfer function approach because it requires very long period Fourier components to reproduce the step function.

5.4. Case Studies

[33] Comparing 663 days of daytime zonal electric field measurements with the transfer function–predicted zonal electric field, *Manoj et al*. [2008] found that the prompt-penetration model can explain about 30% of the non-climatological variation in the electric field data. We apply the updated transfer function to predict the EEF variations correlated to the IEF on 2 days (Figure 7).

[34] The average *ap* index for the day was 24.6. Two main IEF perturbations were between 5–8 and 14–18 UT. The EEF in the Indian sector showed simultaneous positive changes with that of the IEF starting at 5 UT (9:30 LT). The observed EEF is matched by the prediction of the model. The IEF perturbations starting at 14 UT has fluctuation periodicity around 2 h—when the prompt penetration is most efficient. In the South American sector, the penetration effect of this signal is evident starting from 8 LT. The model-predicted EEF matches reasonably with the observation. The JULIA-derived EEF data show a positive increase at 8 LT, in response to the changes in the IEF at 13 UT. However, the model-predicted EEF slightly underestimates the actual variation (Figure 8).

[35] On this day, IEF variations show high-frequency variations, mostly with periodicities less than 2 h. The IEF fluctuations with amplitudes within ±5 mV/m penetrate to the EEF starting at 3 UT. The EEF data from the Indian sector show correlated signals with an amplitude of ±0.2 mV/m. The model prediction matches with the observed data. The model seems overestimating the EEF trough at 11:30 LT. The JULIA EEF data at the South American sector for the same day show a series of penetration electric field that is correlated with the IEF data starting at 9 LT (14 UT). Again, the predicted EEF matches with the data. However, the rapid changes in EEF shown by the JULIA data between 7 and 8 LT are not predicted by the model. As we discussed before, the average transfer function has low admittance for fluctuations with periodicities less than 30 min.

6. Summary and Conclusions

[36] We investigated the spectra of the equatorial ionospheric eastward electric field in the periods from 30 min to 512 h. Our EEF data were derived from the CHAMP scalar magnetometer data and the JULIA radar data acquired during

the years 2000–2009. The slow local time progression of CHAMP provided us with a new opportunity to study the EEF frequency spectra for periods greater than 6 h for the first time. We also addressed the important question about the longevity of the prompt-penetration effects in the equatorial ionosphere using joint signal analysis of the EEF with the coincident interplanetary electric field data. Finally, we updated and validated our transfer function model [*Manoj et al.*, 2008] by incorporating the CHAMP-derived coefficients for periods greater than about 6 h. The major results from this work are summarized below.

[37] 1. The power spectral density of the EEF derived from the JULIA radar and CHAMP magnetic measurements show good agreement at the period of about 6 h. The continuity in spectra validates our spectral estimation method from the CHAMP data.

[38] 2. When $ap > 20$, and for periods between 30 min and 2 h, the slope of the EEF spectra is significantly higher than that of the IEF. Above 2 h, the EEF spectra quickly return to the average background trend. This is also the period range where the IEF and the EEF are most coherent.

[39] 3. From its peak value of 0.7 at 2 h, the coherence quickly decays on either side of the frequency spectrum. Both the CHAMP- and JULIA-derived coherence values are very similar at the period of about 6 h. While the coherence itself is small for this period, the values are statistically significant.

[40] 4. While the background signal power in the EEF is directly related to the geomagnetic activity level, its peaks at 8, 12, 16, and 24 h are not. This means that the atmospheric sources dominate the EEF at these periodicities and that the magnetospheric sources dominate the EEF at periods in between the peaks.

[41] 5. The most dominant spectral peak in the EEF spectra is at 24 h. Beyond 24 h, the spectra suddenly lose power. There are two smaller peaks in the power spectra approximately at 29 and 42 h. There is an increasing trend in the EEF power from about 200 to 512 h, probably due to the left flank of the 27 day (648 h) peak attributed to solar rotation.

[42] 6. The estimated error for the CHAMP transfer function at 6 h is less than that from the JULIA data—mainly due to the higher coherence between CHAMP and IEF at this period. This gives more confidence on the transfer function model for periods greater than about 6 h.

[43] 7. The CHAMP-derived transfer function confirms that the prompt penetration response of the equatorial ionospheric electric field to a 1 mV/m change in the IEF is negligible after 3 h and up to the maximum analysis period of 32 h. This result confirms a previous estimate based only on the JULIA radar data [*Manoj et al.*, 2008].

[44] 8. We have updated the transfer function model with the new data sets and made the filter coefficients available to the scientific community. We also have validated the transfer function model on 2 moderately active days in 2001 and 2002. The predicted EEF matched reasonably well with the observed EEF in both the South American and Indian sectors.

Appendix A: Test of Transfer Function on Mock Data

[45] Our objective here is to demonstrate that our spectral averaging method can reliably estimate the transfer function and its errors between the IEF and the EEF in the presence

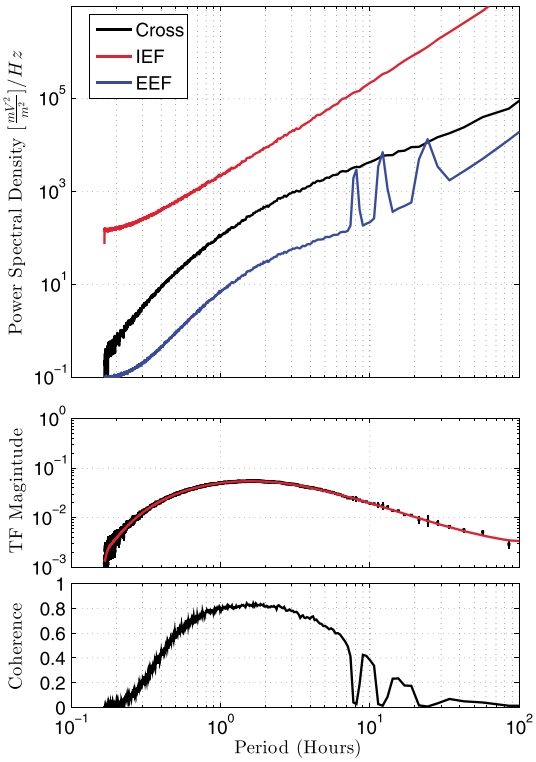

Figure A1. Average spectra of the synthetic interplanetary electric field (red) and the equatorial ionospheric electric field (blue) are plotted on the first panel. Their cross power is plotted in black. The tidal signals in the EEF (peaks at 24, 12, and 8 h) are uncorrelated with the IEF and get averaged out in the cross power. The second panel shows the expected (red) and recovered (black squares) transfer function magnitudes between IEF and EEF. The third panel shows the coherence between IEF and EEF.

of significant uncorrelated noise in the EEF. As we discussed in section 3, the EEF spectra derived from CHAMP show large peaks of tidal signals in the period range where we want to estimate the transfer function. Although it is possible to remove the mean climatological variations (which include the *E* region tides) from the EEF data using the *Alken and Maus* [2010] model, the residuals between the model and the data add up since the autospectra are squared positive quantities. We construct a synthetic time series of the IEF and the EEF, calculate their spectral densities, average their spectra, and, finally, estimate their transfer function and errors. The IEF can be considered as a $^1/_f$ noise since its power increases inversely proportional to the frequency. We first generate a time series with a zero mean Gaussian error and then digitally filter it to provide a slope of -2 on a log-log scale. We then scale it to match the observed IEF data (Figure 3). The EEF data were created similarly, but with a spectral amplitude of about 2 orders less than that of the IEF to match with the observations. Note that the background IEF and EEF are uncorrelated. To the background EEF, we add a prompt-penetration time series predicted from the IEF time series with our transfer function model. Finally, we added three sinusoidal signals with periods of 24, 12, and 8 h to represent the tidal peaks that we observe in the EEF spectra. The time series were sampled at 5 min interval and

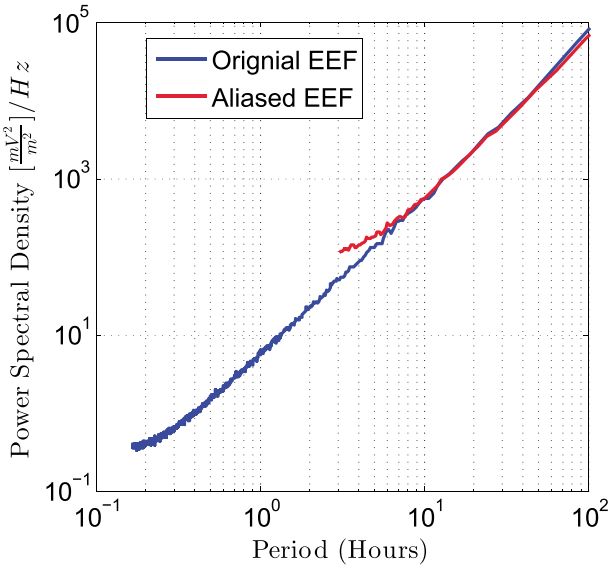

Figure B1. Synthetic EEF spectra from an original sampling interval of 5 min (blue) and the spectra after downsampling the time series every 90 min (red). The resampled spectra show a deviation from the original spectra for periods of 3 to about 6 h. The deviation (known as aliasing effect) is due to the power in the lower periods (lower than the Nyquist frequency of 3 h) folding on to the higher periods. For the analysis of the CHAMP data, we consider only periods of 6 h and above.

were divided into 1000 segments, each with 2048 points. We estimate the cross- and auto–power spectral densities, transfer functions, and coherence of the data sets following the *Welch* [1967] average periodogram method as described in sections 3 and 4.

[46] The spectral densities of the IEF and the EEF are presented in the first panel in Figure A1. Note that both the spectral densities flatten on the lower period as they hit the noise floor. The power spectral density of the EEF (Figure A1, first panel) shows two departures from the background noise. The prompt-penetration signal causes a "bulge" centered at 2 h, and the tidal waves create peaks at 24, 12, and 8 h. However, the crosspower spectral density between IEF and EEF shows only the contribution from the prompt-penetration effect. While the tidal harmonics in the synthetic EEF are significant, they are uncorrelated with the IEF. While the autospectra are real valued and add up both signal and noise, the cross–power spectra are complex values, and the uncorrelated noise with random phase spectra tends to average out with increasing number of segments. It then follows that the influence of noise in the numerator of the transfer function equation 2 can be completely removed with sufficient averaging. This is demonstrated in Figure A1 (second panel), where we compare the magnitudes of the "true" transfer function (red) and the recovered transfer function (black squares). However, we can clearly see the loss of coherence (third panel) and corresponding increases in the transfer function errors in the period ranges where the tidal peaks are present. Spectral averaging improves the variance of coherence but does not restore coherence. The errors in the transfer function magnitude and phase are due primarily to the breakdown in coherence [equations 3 and 4]. For example, where coherence is below 0.1, the transfer function error is about 0.225 times the transfer function magnitude. As equation 4 predicts and Figure A1 demonstrates, the error is a good indicator on the quality of the estimated transfer function.

Appendix B: Aliasing Due to CHAMP

[47] We demonstrate the spectral aliasing effect of the CHAMP-measured EEF using synthetically generated data. We create background EEF data by a procedure similar to that described in Appendix A by sampling every 5 min. We then downsample the time series every 90 min to mimic CHAMP's sampling pattern. We divide the original EEF time series to 2048 points long segments and the downsampled time series to 128 points long segments. We estimate the autopower spectral densities of the data sets following the *Welch* [1967] average periodogram method. Synthetic EEF spectra from the original sampling interval of 5 min (blue) and the spectra after downsampling the time series every 90 min (red) are given in Figure B1. The resampled spectra show a deviation from the original spectra for periods of 3 to about 6 h. The deviation (known as aliasing effect) is due to power in the lower periods (lower than the Nyquist frequency of 3 h) folding on to the higher periods. For the analysis of the CHAMP data, we consider only periods of 6 h and above.

[48] **Acknowledgments.** We acknowledge the OMNIWEB service by NASA for access to the solar wind measurements data. The Jicamarca Radio Observatory is a facility of the Instituto Geofisíco del Perú operated with support from the NSF Cooperative Agreement ATM-0432565 through Cornell University. The Indian geomagnetic observatories ABG and TIR are operated by the Indian Institute of Geomagnetism. The operational support of the CHAMP mission by the German Aerospace Center (DLR) and the financial support for the data processing by the Federal Ministry of Education and Research (BMBF) are gratefully acknowledged. Comments by Janet Machol of NOAA improved the manuscript.

[49] Robert Lysak thanks the reviewers for their assistance in evaluating this paper.

References

Alken, P., and S. Maus (2010), Electric fields in the equatorial ionosphere derived from CHAMP satellite magnetic field measurements, *J. Atmos. Sol. Terr. Phys.*, *72*(4), 319–326.

Anderson, D., A. Anghel, J. Chau, and O. Veliz (2004), Daytime vertical E x B drift velocities inferred from ground-based magnetometer observations at low latitudes, *Space Weather*, *2*, S11001, doi:10.1029/2004SW000095.

Earle, G. D., and M. C. Kelley (1987), Spectral studies of the sources of ionospheric electric fields, *J. Geophys. Res.*, *92*(A1), 213–224.

England, S. L., S. Maus, T. J. Immel, and S. B. Mende (2006), Longitudinal variation of the E-region electric fields caused by atmospheric tides, *Geophys. Res. Lett.*, *33*, L21105, doi:10.1029/2006GL027465.

Huang, C. S., J. C. Foster, and M. C. Kelley (2005), Long-duration penetration of the interplanetary electric field to the low-latitude ionosphere during the main phase of magnetic storms, *J. Geophys. Res.*, *110*, A11309, doi:10.1029/2005JA011202.

Huang, C. S., S. Sazykin, J. L. Chau, N. Maruyama, and M. C. Kelley (2007), Penetration electric fields: Efficiency and characteristic time scale, *J. Atmos. Sol. Terr. Phys.*, *69*(10), 1135–1146.

Hysell, D. L., M. F. Larsen, and R. F. Woodman (1997), JULIA radar studies of electric fields in the equatorial electrojet, *Geophys. Res. Lett.*, *24*, 1687–1690.

Kelley, M. C. (1989), *The Earth's Ionosphere: Plasma Physics and Electrodynamic*, Academic, San Diego, Calif.

Kelley, M. C., J. J. Makela, J. L. Chau, and M. J. Nicolls (2003), Penetration of the solar wind electric field into the magnetosphere/ionosphere system, *Geophys. Res. Lett.*, *30*(4), 1158, doi:10.1029/2002GL016321.

Kirchner, J. W. (2005), Aliasing in 1/ f^{α} noise spectra: Origins, consequences, and remedies, *Phys. Rev. E*, *71*(6), 066110.

Kudeki, E., and C. D. Fawcett (1993), High resolution observations of 150 km echoes at Jicamarca, *Geophys. Res. Lett.*, *20*(18), 1987–1990.

Kudeki, E., C. D. Fawcett, W. L. Ecklund, P. E. Johnston, and S. J. Franke (1998), Equatorial 150-km irregularities observed at Pohnpei, *Geophys. Res. Lett.*, *25*(21), 4079–4082.

Li, G., B. Miao, Q. Hu, and G. Qin (2011), Effect of current sheets on the solar wind magnetic field power spectrum from the ulysses observation: from Kraichnan to Kolmogorov scaling, *Phys. Rev. Lett.*, *106*, 125001.

Lühr, H., S. Maus, and M. Rother (2004), Noon-time equatorial electrojet: Its spatial features as determined by the CHAMP satellite, *J. Geophys. Res.*, *109*, A01306, doi:10.1029/2002JA009656.

Lühr, H., M. Rother, K. Häusler, B. Fejer, and P. Alken (2012), Direct comparison of nonmigrating tidal signatures in the electrojet, vertical plasma drift and equatorial ionization anomaly, *J. Atmos. Sol. Terr. Phys.*, *75*, 31–43.

Manoj, C., and S. Maus (2012), A real-time forecast service for the ionospheric equatorial zonal electric field, *Space Weather*, *10*, S09002, doi:10.1029/2012SW000825.

Manoj, C., H. Lühr, S. Maus, and N. Nagarajan (2006), Evidence for short spatial correlation lengths of the noontime equatorial electrojet inferred from a comparison of satellite and ground magnetic data, *J. Geophys. Res.*, *111*, A11312, doi:10.1029/2006JA011855.

Manoj, C., S. Maus, H. Lühr, and P. Alken (2008), Penetration characteristics of the interplanetary electric field to the daytime equatorial ionosphere, *J. Geophys. Res.*, *113*, A12310, doi:10.1029/2008JA013381.

Maruyama, N., A. D. Richmond, T. J. Fuller-Rowell, M. V. Codrescu, S. Sazykin, F. R. Toffoletto, R. W. Spiro, and G. H. Millward (2005), Interaction between direct penetration and disturbance dynamo electric fields in the storm-time equatorial ionosphere, *Geophys. Res. Lett.*, *32*, L17105, doi:10.1029/2005GL023763.

Meyer-Vernet, N. (2007), *Basics of the Solar Wind*, Cambridge Univ. Press, Cambridge, U.K.

Mursula, K., and B. Zieger (1996), The 13.5-day periodicity in the Sun, solar wind, and geomagnetic activity: The last three solar cycles, *J. Geophys. Res.*, *101*(A12), 27,077–27,090, doi:10.1029/96JA02470.

Nicolls, M. J., M. C. Kelley, J. L. Chau, O. Veliz, D. Anderson, and A. Anghel (2007), The spectral properties of low latitude daytime electric fields inferred from magnetometer observations, *J. Atmos. Sol. Terr. Phys.*, *69*(10–11), 1160–1173.

Nishida, A. (1968), Coherence of geomagnetic DP 2 fluctuations with interplanetary magnetic variations, *J. Geophys. Res.*, *73*(17), 5549–5559.

Reigber, C., H. Lühr, and P. Schwintzer (2002), CHAMP mission status, *Adv. Space Res.*, *30*(2), 129–134.

Russell, C. T. (1972), Comments on the measurement of power spectra of the interplanetary magnetic field, *Solar Wind*, NASA Spec. Publ. 308, pp. 365–374.

Salby, M. L. (1982), Sampling theory for asynoptic satellite observations. Part I: Space-time spectra, resolution, and aliasing, *J. Atmos. Sci.*, *39*(11), 2577–2600.

Sari, J. W., and N. F. Ness (1969), Power spectra of the interplanetary magnetic field, *Solar Phys.*, *8*(1), 155–165.

Scherliess, L., and B. G. Fejer (1999), Radar and satellite global equatorial F region vertical drift model, *J. Geophys. Res.*, *104*(A4), 6829–6842, doi:10.1029/1999JA900025.

Smith, J. O. (2007), *Introduction to Digital Filters with Audio Applications*, online book, Stanford University, Stanford, Calif. (Available at https://ccrma.stanford.edu/~jos/filters/ [last accessed on April 1, 2013])

Swanson, D. C. (2000), *Signal Processing for Intelligent Sensor Systems*, Marcel Dekker, New York.

Thompson, R. O. (1979), Coherence significance levels, *J. Atmos. Sci.*, *36*, 2020–2021.

Titheridge, J. E. (1973), The electron content of the southern mid-latitude ionosphere, 1965–1971, *J. Atmos. Terr. Phys.*, *35*(5), 981–1001.

Vasyliunas, V. M. (1972), The interrelationship of magnetospheric processes, in *Earth's Magnetosphere Processes*, edited by M. McCormac, pp. 29–38, D. Reidel, Norwell, Mass.

Welch, P. (1967), The use of fast Fourier transform for the estimation of power spectra: A method based on time averaging over short, modified periodograms, *IEEE Trans. Audio Electroacoust.*, *15*(2), 70–73.